


RESEARCH ARTICLE | DECEMBER 04 2018

Dimensional variation of reconfigurable serpentine graphene nanoribbon under tension

Yafei Wang; Changguo Wang ; Yunce Zhang; Jiaming Guo; Huifeng Tan



J. Appl. Phys. 125, 082509 (2019)

<https://doi.org/10.1063/1.5050458>



Articles You May Be Interested In

Microstructured electrodes supported on serpentine interconnects for stretchable electronics

APL Mater. (February 2019)

Pre-patterned ZnO nanoribbons on soft substrates for stretchable energy harvesting applications

J. Appl. Phys. (May 2013)

Investigation of the thermal conductivity of shape-modulated silicon nanowires by the Monte Carlo method combined with Green–Kubo formalism

Appl. Phys. Lett. (June 2024)



Nanotechnology & Materials Science



Optics & Photonics



Impedance Analysis



Scanning Probe Microscopy



Sensors



Failure Analysis & Semiconductors



Unlock the Full Spectrum.
From DC to 8.5 GHz.

Your Application. Measured.

Find out more



Dimensional variation of reconfigurable serpentine graphene nanoribbon under tension

Cite as: J. Appl. Phys. **125**, 082509 (2019); doi: [10.1063/1.5050458](https://doi.org/10.1063/1.5050458)

Submitted: 31 July 2018 · Accepted: 4 November 2018 ·

Published Online: 4 December 2018



Yafei Wang,^{1,2} Changguo Wang,^{1,2,a)} Yunce Zhang,^{1,3} Jiaming Guo,^{1,2} and Huifeng Tan^{1,2}

AFFILIATIONS

¹Center for Composite Materials, Harbin Institute of Technology, Harbin 150001, People's Republic of China

²National Key Laboratory of Science and Technology on Advanced Composites in Special Environments, Harbin Institute of Technology, Harbin 150080, People's Republic of China

³College of Aerospace and Civil Engineering, Harbin Engineering University, Harbin 150001, People's Republic of China

^{a)}Author to whom correspondence should be addressed: wangcg@hit.edu.cn

ABSTRACT

In this paper, we resort to single-layer graphene nanoribbon (GN) and atomistic simulation to explore the dimensional variation of serpentine graphene. A tensile model of serpentine GN is established, and its topology responses are investigated with some counterintuitive expectations. A laser scanning experiment on the serpentine sheet of paper is performed and compared, which can indirectly reflect the reduced-dimensionality tendency of serpentine GN in tension. As a result, serpentine GN provides dynamic route of transforming lateral and longitudinal dimensions. Our obtained results can be used to the thermal, electric, or magnetic controlling in future applications.

Published by AIP Publishing. <https://doi.org/10.1063/1.5050458>

I. INTRODUCTION

Three-dimensional (3D) reconfigurable mesostructures induced by compressive buckling^{1–5} have recently sparked great attention due to their topological shapes and tunable dimensions. A programmable design of two-dimensional (2D) precursors can generate tunable 3D mesoscopic configurations determinately that can potentially be exploited in a variety of applications such as self-propelled microrobots,⁶ soft electronics,⁷ and reconfigurable metamaterial,⁸ among others. These 3D reconfigurable mesostructures can be divided into four typical categories⁹ including 3D filamentary structures,¹ 3D kirigami-inspired structures,² 3D origami-inspired structures,³ and 3D dense architectures with entangled layouts.⁵ Although wide length scales of 3D reconfigurable structures can be implemented from submicron to meter dimensions, reducing the lateral dimensions to nanoscales⁹ will give 3D structures a remarkably versatile ability.

Among the many attractive 2D materials, the extraordinary mechanical,¹⁰ electrical,¹¹ and thermal¹² properties of graphene may permit it having a high-level versatility at nanoscales, making graphene an excellent candidate for a variety of applications, such as nanocomposites,¹³ nanomechanical resonators,¹⁴

thermal nanomodulators,^{15,16} and nanoelectromechanical systems.¹⁷ Accompanying the rapid development of manufacturing techniques, photolithography, sonochemical methods, thin film etching, templated growth, and self-assembly will be applied to excised geometry of 2D materials^{18,19} and assemble them in nanomechanical systems determinately. It is possible to make use of the 2D excised graphene nanoribbons (GNs) to demonstrate the scalability of 3D reconfigurable structures at nanoscales and the feasibility of reducing the lateral dimensions of 3D structures to nanoscales.

Despite the latest scientific advances, certain limitations and constraints remain. Up to now, most concerns have been focused on compressive buckling induced 3D reconfigurable mesostructures by the finite element method (FEM).^{1–3,5} This is because the compressive force of substrates impels the 2D precursors to exist in the state-of-the-art 2D microsystem to transform a flat 2D configuration into a 3D topological elaborated structure. This idea is well-implemented via prestrain and releasing mechanism of elastic substrate. According to the inverse considerations, the tensile mechanism can also be exploited in generating out-of-plane buckling of a sophisticated material, which can transform 2D materials into complex

configurations. For instance, Rafsanjani and Bertoldi²⁰ investigated the mechanical response of thin sheets perforated with a square array of mutually orthogonal cuts using analytical, experimental, and numerical methods. They demonstrate that, under uniaxial tension, the ligaments of a perforated thin sheet will buckle out of plane and the formation of periodic 3D patterns is controlled by the load direction. Furthermore, one of the attractive advantages of 3D reconfigurable structures is that they can be exploited in a broad range from submicron to meter dimensions. Subsequently, validation of 3D structures at the nanoscale is an urgent need, as these advances provide a potent guide to an experimentalist or a scientist in designing state-of-the-art nanodevices. To the best of our knowledge, few efforts are devoted to study the topological reconfigurable nanostructures of low-dimensional materials (such as graphene, the most studied 2D material). Song *et al.*²¹ reported a new methodology to create periodic 3D origami patterns out of silicon nanomembranes using prestrain and prepatterned polydimethylsiloxane (PDMS) substrates. But the Si origami they described belongs to microscale, and the microscale 2D precursor has to be supported by a substrate. From a methodological point of view, correspondingly appropriate techniques should be implemented to capture the topological structures with respect to different scales. For example, Xu *et al.*¹ utilized FEM to quantitatively predict the assembly of 3D filamentary mesostructures, and the simulation results are in good agreement with the experiments. Whereas for many important findings, atomistic simulations can be considered as a promising approach for the design of tailed graphene structures with optimized performance, and the accurate description of molecular dynamics is an essential theoretical tool for studying the mechanical or other physical responses of graphene at nanoscales. Qin *et al.*²² demonstrated that the interlayer shear mechanical properties of freestanding graphene with topographical defects can be significantly increased based on atomistic simulations, and the curved surface due to out-of-plane wrinkles can be characterized by a sinusoidal surface. Qi *et al.*²³ in their classical molecular dynamics simulations reported that the yield and fracture of graphene kirigami can be enhanced by about 3 times relative to pristine graphene, while they give special attention to the mechanical response of graphene kirigami under tensile strain. Mortazavi *et al.*²⁴ performed extensive atomistic simulations to explore the thermal and electrical transport characteristics of highly stretchable graphene kirigami. They found that the periodic 2D graphene kirigami presents highly anisotropic thermal and electrical transport.

In general, 3D reconfigurable structures have attracted exceptional attention and leveraged the 2D materials to transform planar thin sheets into 3D sculptures. While the studies on 3D reconfigurable structures are still limited to compressive buckling mechanism, very few efforts were devoted to study the reconfiguration of graphene (the most studied 2D material to date) at nanoscales. Toward this end, utilizing advanced materials with the support of atomistic simulations to expand the available dimensions of 3D reconfigurable structures at nanoscale levels is the motif in this research.

In this work, serpentine graphene nanoribbon, a kirigami-inspired structure, is designated to investigate its dimensional variations under tension. The remainder of this paper is organized as follows. In Sec. II, we describe our molecular model and simulation methods. In Sec. III, we analyze and discuss the analytical results of 3D serpentine GNs. De-wrinkling effect, domino rippling effect, reduced-dimensionality tendency, and metalinking effect of serpentine GN under tensile strain are also unveiled in this section. In Sec. IV, we recap our motif and end with a summary of the results.

II. MODEL AND METHODS

Inspired by recent experimental²⁵ and theoretical²⁶ researches on serpentine graphene that the bandgap of narrow GNs with widths less than 2 nm could be comparable to that in silicon (1.1 eV), we recur to graphene “kirigami” technology, where serpentine graphene with customizable lateral dimensions can be implemented in Fig. 1. Unlike freestanding GN, two pairs of clamps are placed at both ends of graphene, free boundary condition (see zigzag chirality in Fig. 1) is used in the X direction. This is because the end-supported GN with the minimizing deleterious substrate effects²⁷ is a promising fundamental element for next-generation nanodevices, and the nanoribbons can be excised with desired motifs before and after putting them onto the clamps.²⁷ Several key geometric parameters²³ of serpentine GN include length of interior cut $B = 36.2 \text{ \AA}$, width of interior cut $C = 9.8 \text{ \AA}$, and distance between two interior cuts $D = 44.2 \text{ \AA}$. A loading method of quasi-static axial tension is carried out to capture 3D configurations. A reversible program is used to realize the reconfigurable surface of serpentine graphene in the valid scope of a tensile load. Importantly for potential uses of this tunable nanomechanical system, design paradigms of 3D serpentine graphene are robust to the change in heat transfer path and stress distribution.

Extensive atomistic simulations were performed to explore the 3D reconfigurable nanostructures using the molecular dynamics engine LAMMPS.²⁸ Considering the reliable prediction of large strain mechanical response^{23,29,30} and bond breaking or reforming of graphene,^{29–32} the second generation REBO potential energy function is used to describe the interatomic interaction among carbon atoms.³³ For the cutoff distance of REBO force field, it should be adjusted to 0.192–0.2 nm to avoid the spurious strengthening effect,³¹ which gets consistent results with our previous works^{16,34} and quantum mechanics calculations.^{19,29,32} In the tensile model for excised graphene,

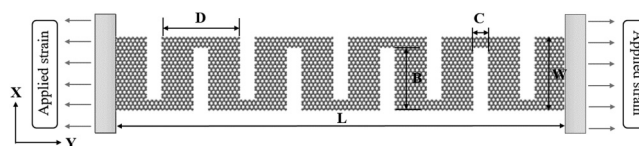


FIG. 1. Tensile model of end-supported 3D serpentine GN with the key geometric parameters. Axial tension is applied at both ends of GN with two pairs of clamps, whose directions are indicated by arrows.

nonperiodic boundary conditions are imposed on all three directions, and an NVT (constant number of particles, constant volume, and constant temperature) ensemble based on the Nosé-Hoover thermostat is employed with a target temperature 0.1K. A time step of 1fs with velocity-Verlet integration algorithm is used in the current simulation. Prior to the atomistic simulations of axial tension, serpentine GN is first optimized to a local minimum configuration via the conjugated gradient algorithm. Subsequently, the relaxation of serpentine GN is carried out with a simulation time 200 ps based on the size of the simulation system and temperature. To ensure that 200 ps is a sufficient equilibrium time, we perform another equilibrium simulation with 1000 ps at 0.1K; the result of equilibrium configuration is similar to the 200 ps equilibration. So we designate 200 ps to conserve computational resources. In addition, the low temperature 0.1K is designated for axial tension to eliminate thermal perturbation. Thus, the results obtained in current research are only valid for temperatures near 0.1K. Simulated axial tension is performed on the equilibrium serpentine GN model with a tensile displacement (velocity) of 0.02 nm/ps in the Y direction. The velocity of -0.01 nm/ps is applied on the left end, while the other end is designated as a velocity of 0.01 nm/ps. The corresponding strain rate of tensile process is 0.00077 ps^{-1} . Strain rates of 0.001 ps^{-1} have been demonstrated to give results which include negligible dynamic effects in graphene nanoribbons.³⁵ Therefore, the strain rate effects (dynamic effects) are insignificant. Due to the limitation of the time scale of atomistic simulations, this set of loading conditions have already offered satisfied prediction corresponding to the real experimental conditions.³⁶

III. RESULTS AND DISCUSSION

A. Edge-material-driven mechanism

Insights from the kirigami arts suggest that some additive properties can be achieved by combining geometric features and intrinsic physical features, where geometry features are mainly related to the tensile effects and rotational effects. For traditional design principles of excised pattern, intermediate excised 2D materials make every segment with respect to each other discrete. It directly leads to the relatively low robustness in bearing the overloaded tensions and rotations in plane or out of plane. Additionally, due to the formation of intermediate vacancies, a large magnitude of phonon scattering will occur at the vacancy edges and intrinsic edges. Hence, a different way should be considered to acquire a more successive motif, as we demonstrated in this work. For a GN with the specific length, deeply excised GN ($0 < 2B/W - 1 < 1$) along both edges, namely serpentine graphene nanoribbons, may showcase the full potential in two main aspects. Firstly, serpentine GN is an effective way to realize the edge-material-driven mechanism. Due to the intrinsic geometrical feature, the straightening process allows extra materials from the edge of GN to swarm into the central region. This is our core design approach. Secondly, serpentine GN can easily realize the continuity of materials, to some extent, and

serpentine GN still belongs to the domain of pristine graphene. The close connection between neighboring segments permits excessive tension or rotation. As for the significant change of transport path and stressful path, the enhancement of stretchability, the variation in phonon scattering, the abnormal variation of stiffness as well as 3D topological reconfiguration, and so on, they may result from intermediary between the peculiar geometrical features and desired functionalities. As a welfare, the resultant topology response of serpentine GN will be systematically demonstrated in this paper. Further exploration may aim at developing the application scope for the field.

B. Lateral dimensional variation

A tensile model of serpentine GN can be proposed to achieve a dynamic route of reducing lateral dimensions. To emphasize the dynamic change with the applied tensile strain, the variation in the lateral dimension is studied firstly. We give a definition of the lateral dimension parameter to demonstrate the magnitude change

$$v_{lx} = -\frac{\varepsilon_x}{\varepsilon_y}. \quad (1)$$

Here, v_{lx} represents the lateral dimension parameter. And corresponding to the applied tensile strain $\varepsilon_y = \varepsilon$ in the Y direction, the resulting strain in the X direction is $\varepsilon_x = (\delta - \delta_0)/\delta_0$, where δ_0 is the original width of GN after equilibration and lateral width is $\delta = x_{\max} - x_{\min}$, x_{\max} and x_{\min} are the maximum and minimum X-coordinate for the simulation system, respectively. Figure 2 depicts the variation in the lateral dimension parameter as a function of tensile strain for the 3D serpentine GN. Generally, Fig. 2 demonstrates that the variation in the lateral

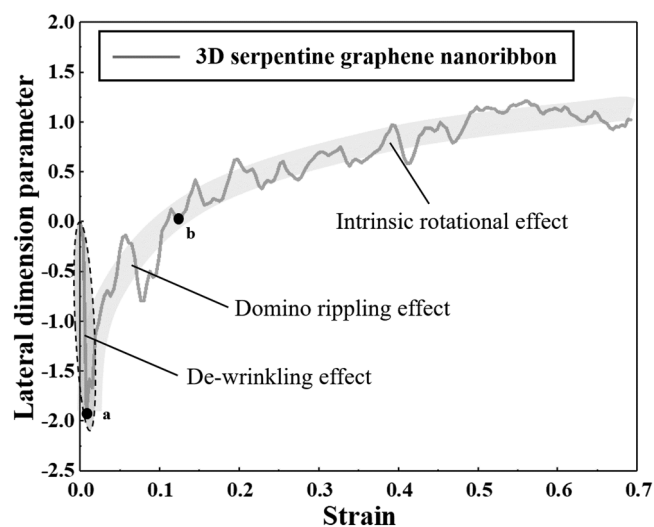


FIG. 2. Strain dependence for the lateral dimension parameter in serpentine GN.

dimension parameter possesses three straightforward regimes. The first regime is formed before critical point a, which is corresponding to the critical tensile strain of 0.0076. It is found that the negative lateral dimension parameter significantly decreases during the small tensile strain. Here, it is important to realize the auxetic effect is robust, as the auxetic behavior is probed for serpentine GN with tensile strain smaller than 0.0076 attaining as large as -1.91 . To unravel the robustness of ν_{lx} as well as the transition of topological configuration, it is helpful to understand the de-wrinkling effect in GN. Due to the edge effect, the characteristic phenomenon for pristine graphene is that the free edges are in their warped state. Mathematically, the edge-stress-driven warped configuration can be described as follows:

$$z = A_0 e^{-\frac{x}{l_c}} \sin\left(\frac{\pi y}{\lambda_0}\right), \quad (2)$$

where A_0 is the wrinkling amplitude of graphene edge, l_c is the penetration depth, and λ_0 is the wrinkling wavelength of the edge. On the other hand, for serpentine GN in this research, increasing the length of the exposed edge makes it possible to attain several degenerate mode shapes with respect to armchair and zigzag chiralities, as we can see from Fig. 3. Different edges of excised GN can stochastically warp with respect to the positive or negative out of plane perturbation [in general, each soliton satisfies the surface function described in Eq. (2)]; however, these perturbations will definitely occur in specific regions of serpentine GN after initial equilibrium. With this edge-stress-driven topological configuration (see Fig. 3) in hand, it is easy to think of auxetic behavior under uniaxial tension, which results from a de-wrinkling mechanism. And the dominant status of de-wrinkling effect

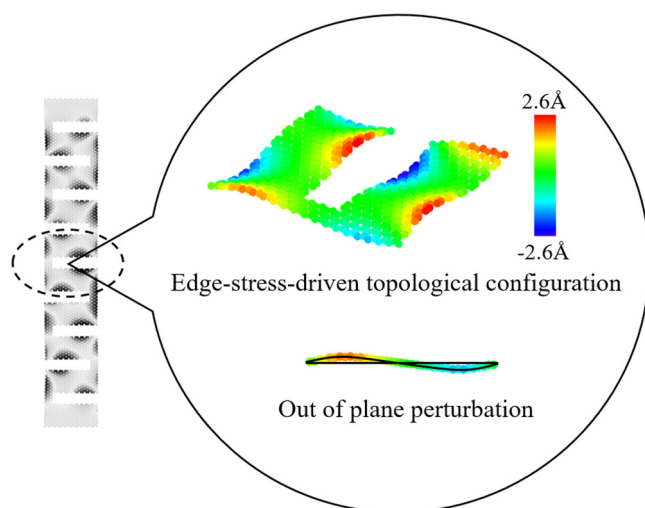


FIG. 3. Edge-stress-driven topological configuration for serpentine GN after the initial equilibrium.

leads to the significant decrease for tensile strain smaller than 0.76%.

At the critical point of a ($\nu_{lx} = -1.91$), we observe that serpentine GN exhibits a topological surface with the Gaussian curvature. This is because the allowed fusions can be realized by two adjacent solitons due to the de-wrinkling effect. These perturbations create favorable conditions to let serpentine GN ripple out of plane. As depicted in Fig. 2, when tensile strain goes into the second regime ($0.0076 < \epsilon < 0.1573$), the lateral dimension parameter increases nonlinearly from the critical point a ($\nu_{lx} = -1.91$) to critical point b (the value of ν_{lx} is about zero). To investigate the strain dependence for ν_{lx} and topological response, typical snapshots of deformation transition in serpentine GN are specifically captured in this regime. From the results shown in Fig. 4(a), it is observed that once the localized point 1 of Gaussian curvature ripples first, the successive rippling of the neighboring segments will be triggered. We use a dominolike rippling effect to describe this successive rippling phenomenon. The propagation of domino wave along the Y direction can be found accordingly [see localized point 1 to localized point 4 in Fig. 4(a)]. With the domino rippling of segments, lateral contraction of excised GN occurs and consequently leads to a slight increase of the lateral dimension parameter. For a negative value of ν_{lx} , our interest is the magnitude change of lateral dimensionality, while it is useful to understand the strong correlations between dominolike successive rippling and common dominoes.³⁷ We know that the energy source of common dominoes is gravitational potential energy, and total potential energy of a system is almost the same after the first collapse reached.³⁷ This is because successive transitions of gravitational potential energy in neighboring elements with respect to each other are enough to maintain a relatively stable energy level. Fortunately, we also find a similar energy state in the 3D excised GN system to give a reasonable analogy. The variation in system potential energy is clearly plotted in Fig. 4(b) (the failure will be initiated when strain is larger than 0.6943). For $0.0076 < \epsilon < 0.1573$, the system potential energy remains almost unchanged, and the value is in a relatively low level after the initial energy minimization. This underlying relationship provides a profoundly physical insight apart from a simple phenomenological resemblance. In addition, we have observed a successive rotational mechanism as described in Fig. 4(a). Domino rippling effect enables a low energy rotational deformation³⁰ in excised GN. Notably, in contrast to high energy stretching³⁰ of intrinsic rotational effect in the final regime [see Fig. 4(b)], domino rippling is more favorable than that of in the third regime.

We note that the propagation speed of domino wave along the Y direction decreases nonlinearly with an increase in tensile strain [see Fig. 4(a)], and the results of domino rippling are independent of loading rate for the quasi-static loading. The whole domino rippling developing will be finished in the second regime. Topological response relative to the lateral dimension experiences a transition from youth period to maturity period. That is, after the bifurcation of $\epsilon = 0.1573$, tensile strain becomes more and more sufficient to cause the recovery

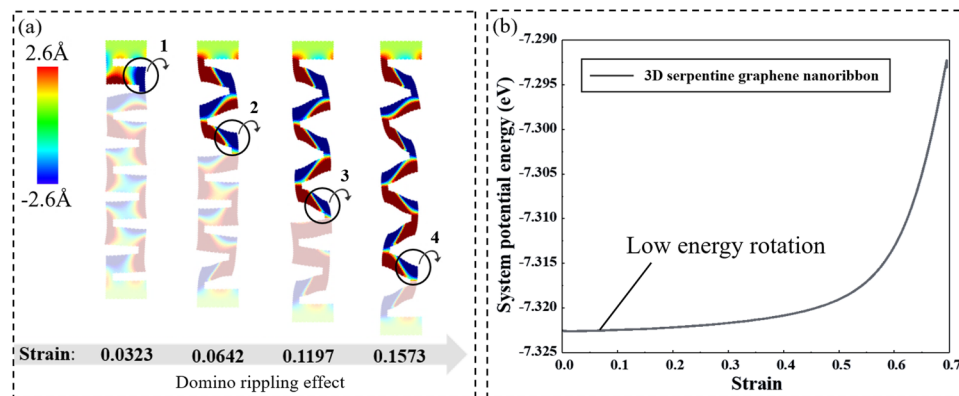


FIG. 4. (a) Snapshots of domino rippling effect for serpentine GN ($0.0323 < \epsilon < 0.1573$), where the color bar is the displacement (Z direction) from -2.6 \AA to 2.6 \AA . (b) Effect of tensile strain on system potential energy in 3D serpentine GN.

and increase of the lateral dimension parameter. Both lateral width and ϵ_x of serpentine GN decrease with increasing tensile strain in the final regime in Fig. 5(a). However, extraordinarily excessive contraction of the lateral direction makes it so different from a serpentine sheet of paper in macroscale. We

designate a lateral rotational angle in Fig. 5(a) to qualitatively characterize the excessive contraction of the lateral dimension. When ϵ_y is from 0.1573 to 0.6460, the lateral rotational angle increases with the applied strain up to 110° . For a serpentine sheet of paper, it is difficult to attain a rotational

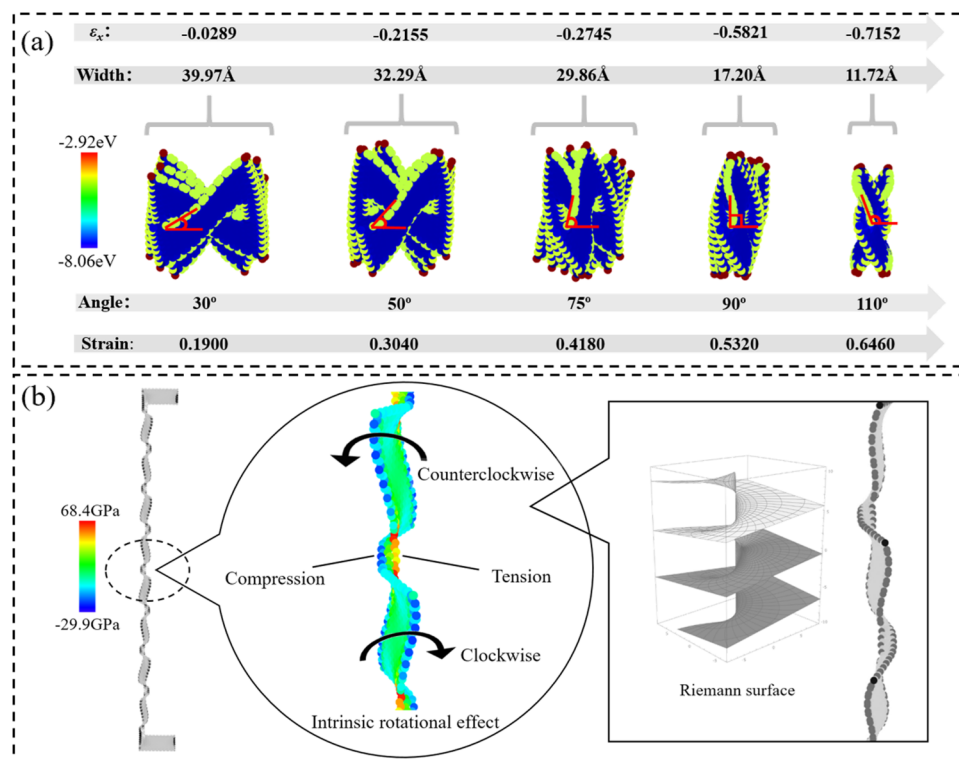


FIG. 5. (a) Evolution of lateral rotational angle ($0.1900 < \epsilon < 0.6460$), where the color bar represents the potential energy. The variation in lateral strain and lateral width is shown in the inset. (b) Intrinsic rotational effect resulting from the asymmetric stress distribution, in which the resultant topological configuration is shaped like a degenerate Riemann surface.

21 April 2025 03:23:13

angle of 90° , let alone up to 110° (lateral rotational angle will continue increasing after $\varepsilon_y = 0.660$). Consequently, this abnormal rotation may emanate from the intrinsic property of GN. To validate our speculation, we firstly refer to the change of system potential energy in Fig. 4(b), and a notable energy enhancement can be observed. This implies that the serpentine GN will again be forced to rotate excessively via a significant high energy stretching. In doing so, the distribution of stress field should be examined to reflect the intrinsic rotational mechanism behind the abnormal increase of lateral rotational angle. In Fig. 5(b), a representative segment of serpentine GN with a strain of 0.6460 is specifically extracted, which the connection ligament in the middle region is in a complex stress state. The tensile stress and compressive stress are mainly distributed on the right side and left side of the connection ligament, respectively. If we specify the ligament surface as the reference plane, the compression-stress-driven portion will immediately buckle out of the reference plane. With the support of high energy stretching on the other side of the ligament, the excessive rotational phenomenon could be observed, which is a relative rotation mode that the top and bottom portions of the segment rotate counterclockwise and clockwise, respectively. Based on the intrinsic rotational effect, other segments will possess a similar deformation mechanism. Interestingly, the resultant topological configuration is shaped like a degenerate Riemann surface, as schematically shown in Fig. 5(b).

C. Longitudinal dimensional variation

By examining the variation in the lateral dimension parameter, a dynamic change of 3D reconfigurable serpentine GN in the lateral direction has been demonstrated and divided into three regimes which correspond to three typical deformation mechanisms. The results obtained in this section may give a good guide to other 2D materials. Next, we investigate the properties of the longitudinal dimension for the 3D topological reconfiguration. By resorting to computational simulations, a clearly reduced-dimensionality tendency in serpentine GN can be observed in Fig. 6. In addition, a similar serpentine sheet of paper, as mentioned above, is manually created. For ease of comparison, we use a couple of geometrical parameters to reflect the geometry characteristics, where it can be recorded as $[2B/W - 1, (D - C)/2W]$. For the serpentine configuration studied in this research, both serpentine GN ($W = 41.1 \text{ \AA}$, $L = 260.3 \text{ \AA}$) and paper are recorded as (0.76, 0.42), and the quasi-static axial tension is carried out to generate the 3D GN. We define an expression of the longitudinal dimension parameter as

$$v_{lz} = \frac{V_z - V_{z0}}{V_{z0}}, \quad (3)$$

where V_z is calculated through the equation $V_z = \left[\sum_{i=2}^N (z_i - \bar{z})^2 / (N - 1) \right]^{1/2}$, V_z is the standard deviation of the Z-coordinates, which can reflect the dispersion degree of the out of plane coordinates. V_{z0} is the initial value of the

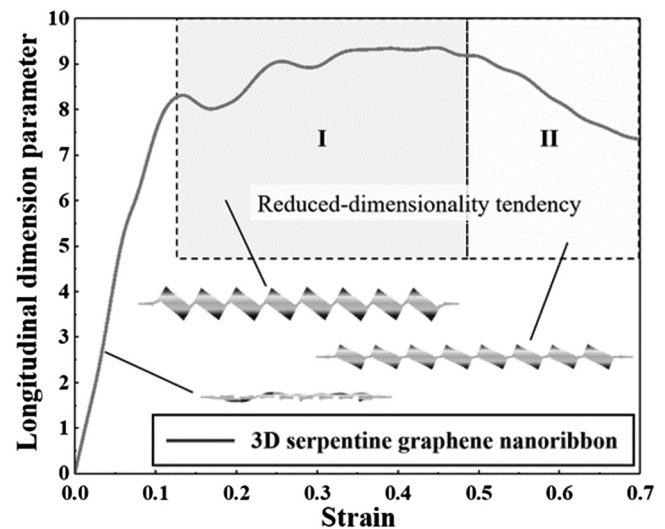


FIG. 6. Reduced-dimensionality tendency of the longitudinal dimension parameter for 3D serpentine GN.

standard deviation, N is the number of atoms or extracted points, z_i is the i -th coordinate in Z direction, and \bar{z} is the average value. As schematically shown in Fig. 6, a reduced tendency of the longitudinal dimension parameter for serpentine GN is observable from stage I to stage II. Based on the analysis of the lateral dimension parameter, we note that the abnormal deflection in Fig. 6 also originates from the intrinsic rotational mechanism of the lateral direction. The finding shows that three dimensionality tendencies exist in serpentine, and one can control the magnitude of dimensionality and configuration state by controlling the strain in a reversible manner. For completeness, the recoverability of serpentine GN is examined in the Appendix.

As mentioned above, we use a 3D scanning technology to achieve the topological configuration of a serpentine sheet of paper described by extracted points, in which the geometry characteristics of serpentine GN and paper could be recorded as $[2B/W - 1, (D - C)/2W] = (0.76, 0.42)$, and the length of serpentine paper is about 45 mm. A 3D laser scanning experiment on the serpentine sheet of paper is performed using a Leica T-Scan laser scanner [see Fig. 7(b)] and a miniature tensile tester [see Figs. 7(c) and 7(d)]; the Leica T-Scan laser scanner is composed of a probing head, a data transformation system, and a data processing system. The specimen is manufactured using excised A4 paper of $210 \times 297 \text{ mm}$. The miniature tensile tester [see Figs. 7(c) and 7(d)] is conducted to realize the quasi-static loading process. Generally speaking, the specimen is carefully clamped with skidproof chunks of the miniature tensile tester with a very slow velocity of 0.0002 m/s [see Fig. 7(c)]. And then the topological response of serpentine paper is measured as precisely as possible with the high-precision probing head [see Fig. 7(d)], for example, we can detect the configuration of serpentine paper every 10 s.

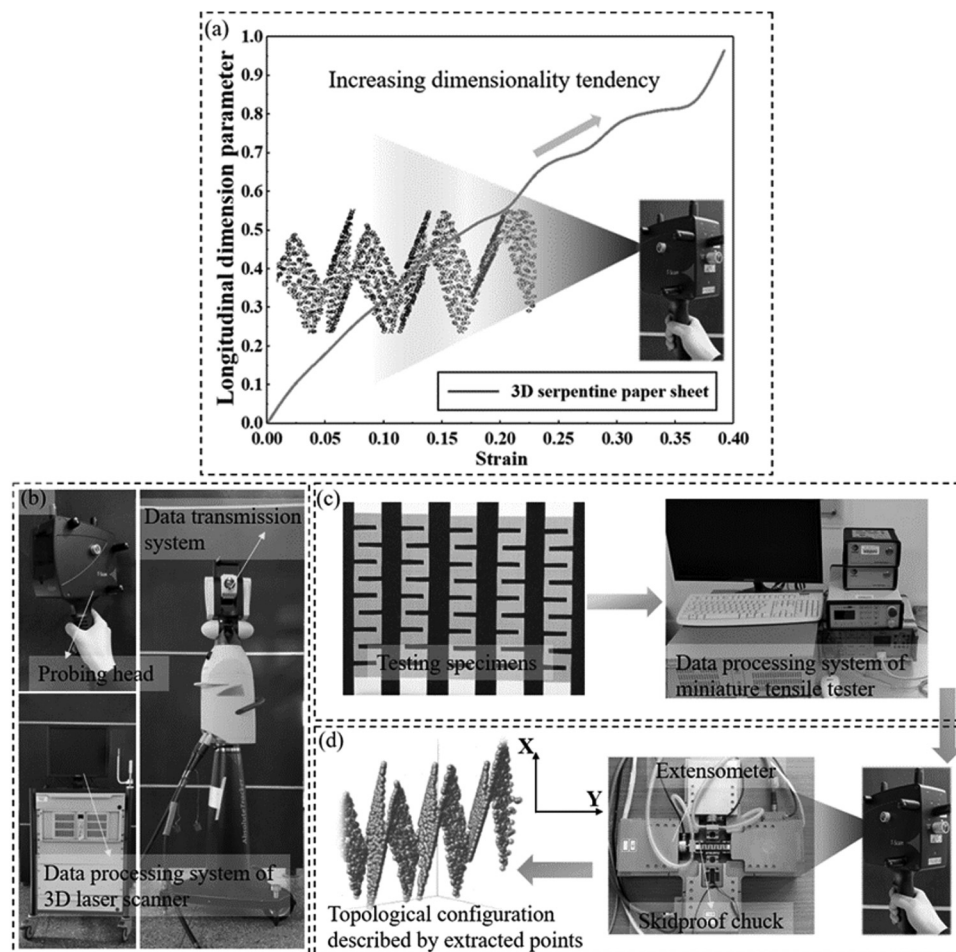


FIG. 7. (a) Increasing dimensionality tendency of longitudinal dimension parameter for the 3D serpentine paper sheet. (b) Leica T-Scan laser scanner (probing head, data transmission system, and data processing system). (c) Five testing specimens and the data processing system of the miniature tensile tester. (d) Probing setup of topological configuration for the testing specimen. And the loading velocity in the Y direction is 0.0002 m/s (the left end is -0.0001 m/s, the right end is 0.0001 m/s). The topological configuration of a serpentine sheet of paper can be described by the extracted points.

Next, the topological configuration of serpentine paper is determined by using a number of extracted points, and these specific points can be transported to the data processing system of the 3D laser scanner. By handling the data properly, we finally achieve a series of topological configurations described by extracted points in the process of quasi-static loading, based on which the longitudinal dimension parameter of serpentine paper can be calculated according to Eq. (3). This process can be realized numerically by using the commercial software MATLAB. Figure 7(a) shows the relationship between longitudinal dimension parameter and tensile strain. Generally, the serpentine paper sheet with the applied tensile strain presents an increasing-dimensionality tendency (longitudinal dimensionality). By probing the lateral rotational angle, we find that the rotational angle attains 90° when tensile strain is equal to 0.3917.

Therefore, the reduced-dimensionality tendency of the longitudinal dimension parameter and the excessive rotational phenomenon may result from the inherent attribute of graphene. And one should note that in this research, we just compare the GN and serpentine paper at the space of dimensionality tendency. Comparing their magnitude of the longitudinal dimension parameter is almost nonsensical here.

D. Metalinking effect

Finally, we realize that there is a latest stage after $\varepsilon = 0.6943$, where it stems from the discussion in how serpentine GN behaves under the ultimate strain. Several previous works demonstrate that carbon exhibits a very abundant dynamic process of bond-breaking and bond-reforming that allows transformations from high dimensional carbon

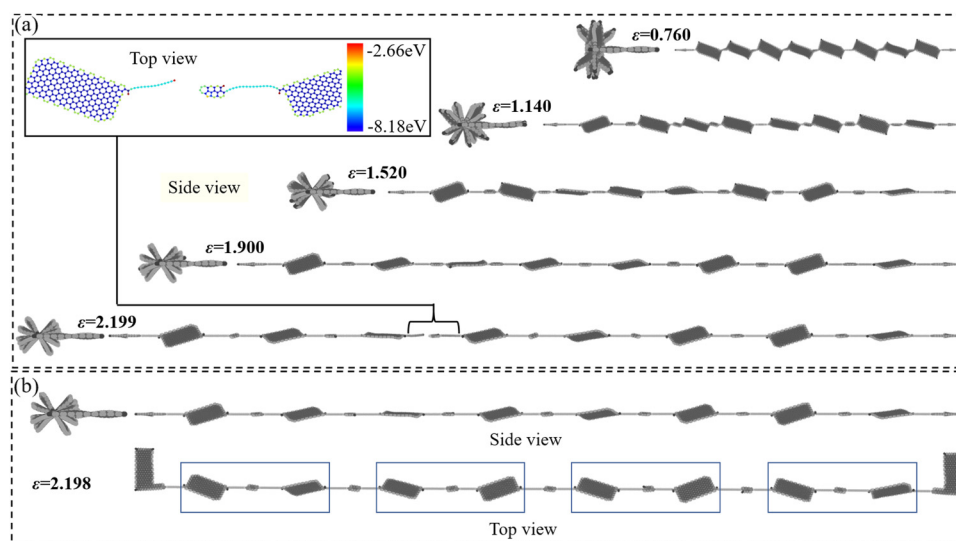


FIG. 8. Snapshots of serpentine GN under the ultimate strain. (a) Several structures obtained by stretching a serpentine GN when $\varepsilon > 0.6943$. The color bar represents the potential energy, which is ranging from -8.18 eV to -2.66 eV; the final fracture site has a higher potential energy. The inset displays the final fracture of 1D carbon chain with respect to the top view. (b) Atomistic and periodic nanostructure of the critical configuration before final fracture. Each box contains two carbon chains with 14 and 17 carbon atoms, respectively.

allotropes to low dimensional carbon allotropes.^{38–41} And Marques et al.³⁹ in their atomistic simulations and high resolution TEM experiments investigated the fracture of nanotubes under high stretching, in which they find the essential role of the vacancies in the lateral dimensional decrease of the nanotube, leading finally to the formation of one-dimensional (1D) carbon chains. These results constitute the evidences of the metalinking phenomenon with the minimal nanowire under high tensile strain,^{38,39} and visualizations of the structural transformations are shown in Fig. 8(a). The variation trend of the longitudinal dimension parameter exactly continues the corresponding trend in Fig. 6. At $\varepsilon = 2.199$, we observe the final fracture of the serpentine GN. The interesting finding is that metalinking configuration tends to break at the end of a 1D carbon chain, which is due to the difference in C–C bond length of metalinking. This special fracture mechanism of 1D carbon chains with sp hybridization is in agreement with the previous experiment and density functional theory (DFT) calculation.⁴¹ We illustrate the critical configuration ($\varepsilon = 2.198$) before final fracture, and an obvious periodical structure can be found in Fig. 8(b). Generally, each box contains two carbon chains with respect to 14 and 17 carbon atoms. By considering the potential application of carbyne in nanoelectronics, nanocomposites, and nanodevices,⁴² this finding may supply a new method for acquiring the minimal nanowire.

IV. CONCLUSION

In summary, we have demonstrated that reconfigurable serpentine GN presents a promising framework in which dimensional variation can be dynamically tuned based on

atomistic simulations. As an additional welfare, the resultant buildup of 3D topological reconfiguration would benefit the exploitation of nanodevices. Several remarkable conclusions are as follows:

- (1) The edge-material-driven mechanism is effective in speed-up of searching the balance point between asymmetric configuration and symmetric configuration.
- (2) The knowledge of the serpentine GN for their topology responses as depicted here can serve as an important building block for modeling other scaled-down approaches and for other topological reconfigurations.
- (3) The influence of edge-stress-driven topological configuration is found to be more robust resulting in a de-wrinkling mechanism. A profoundly physical insight can give a reasonable analogy between domino rippling effect and common dominoes.
- (4) Excessive rotation of lateral rotational angle is due to asymmetric stress distribution of the connection ligament, in which the dual responses of abnormal rotation lead to the intrinsic rotational effect and reduced-dimensionality tendency phenomenon.
- (5) Due to the diversity of carbon bond-breaking and bond-reconstruction, an obvious periodical structure with 1D carbon chains can be formed, which this metalinking effect directly leads to the abnormal final fracture site.

ACKNOWLEDGMENTS

This work was supported by the National Natural Science Foundation of China (NNSFC) (No. 11572099), the Natural

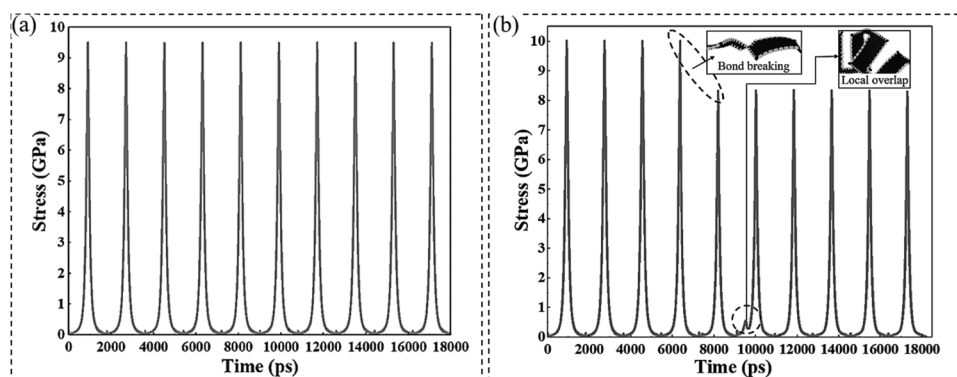


FIG. 9. Tensile loading-unloading curves of serpentine GN over 10 cycles. (a) Reciprocating loadings of serpentine GN. The maximum tensile strain is equal to 0.6840. (b) Tensile curve of reciprocating loadings. The cycle period of serpentine GN is from 0.0000 to 0.6916 to 0.0000. The insets are breaking of carbon bonds and local overlap of GN, respectively.

Science Foundation of Heilongjiang Province of China (No. A2015002), the Fundamental Research Funds for the Central Universities (No. HIT.MKSTISP.2016 29), and the Aeronautical Science Foundation of China (No. 2016ZA77001). The authors wish to thank Mrs. Zaiying Zhang and Mr. Gongran Wang for their thoughtful kindness. The authors would like to express their thanks and appreciation to the anonymous reviewers whose substantial and constructive comment significantly improved the research.

APPENDIX: RECOVERABILITY

As shown in Fig. 9(a), we specify that the maximum tensile strain is as large as 0.6840. It is worth noting that there is no mechanical energy dissipation during the 10 reciprocating loadings. The excellent recoverability can be demonstrated by this computational test. However, if we designate the tensile strain from 0.0000 to 0.6916 to 0.0000 as a cycle period, a significant energy dissipation can be observed after 4 cycle periods [see Fig. 9(b)]. This indicates that the serpentine GN cannot reshape its original configuration and the structural damage occurs in the reconfiguration system after 4 cycle periods. The significant energy dissipation results from the bond breaking of carbon, in which one-dimensional carbon chain is formed at the fracture region. For the 6th loading process, a local overlap of serpentine GN results in the fluctuation of the curve.

REFERENCE

- ¹S. Xu, Z. Yan, K. I. Jang, and W. Huang, *Science* **347**, 154 (2015).
- ²Y. Zhang, Z. Yan, K. Nan, and D. Xiao, *Proc. Natl. Acad. Sci. USA* **112**, 11757 (2015).
- ³Z. Yan, F. Zhang, J. Wang, and F. Liu, *Adv. Funct. Mater.* **26**, 2629 (2016).
- ⁴Y. Liu, Z. Yan, Q. Lin, and X. Guo, *Adv. Funct. Mater.* **26**, 2909 (2016).
- ⁵Z. Yan, F. Zhang, F. Liu, and M. Han, *Sci. Adv.* **2**, e1601014 (2016).
- ⁶Z. Yan, M. Han, Y. Shi, and A. Badea, *Proc. Natl. Acad. Sci. USA* **114**, E9455 (2017).
- ⁷Y. Sun, W. M. Choi, H. Jiang, and Y. Y. Huang, *Nat. Nanotechnol.* **1**(3), 201 (2006); K. I. Jang, K. Li, H. U. Chung, and S. Xu, *Nat. Commun.* **8**, 15894 (2017).
- ⁸J. K. Gansel, M. Thiel, M. S. Rill, and M. Decker, *Science* **325**, 1513 (2009).
- ⁹Z. Yan, M. D. Han, Y. Y. Yang, and K. W. Nan, *Extreme Mech. Lett.* **11**, 96 (2017).
- ¹⁰C. Lee, X. Wei, J. W. Kysar, and J. Hone, *Science* **321**(5887), 385 (2008).
- ¹¹N. M. R. Peres, *Vacuum* **83**, 1248 (2009).
- ¹²S. Ghosh, I. Calizo, D. Teweldebrhan, and E. P. Pokatilov, *Appl. Phys. Lett.* **92**, 151911 (2008).
- ¹³S. Stankovich, D. A. Dikin, G. H. Dommett, and K. M. Kohlhaas, *Nature* **442**, 282 (2006); R. J. Young, I. A. Kinloch, L. Gong, and K. S. Novoselov, *Compos. Sci. Technol.* **72**, 1459 (2012).
- ¹⁴C. Chen, S. Rosenblatt, K. I. Bolotin, W. Kalb, and P. Kim, *Nat. Nanotechnol.* **4**, 861 (2009); J. S. Bunch, A. M. van der Zande, S. S. Verbridge, and I. W. Frank, *Science* **315**, 490 (2007).
- ¹⁵X. J. Liu, G. Zhang, and Y. W. Zhang, *Nano Res.* **8**, 2755 (2015).
- ¹⁶C. Wang, Y. Liu, L. Li, and H. Tan, *Nanoscale* **6**, 5703 (2014).
- ¹⁷V. M. Pereira and A. H. Castro Neto, *Phys. Rev. Lett.* **103**, 046801 (2009).
- ¹⁸Z. H. Wu, W. C. Ren, L. B. Gao, and B. L. Liu, *Nano Res.* **3**(1), 16 (2010); J. Bai, X. Zhong, S. Jiang, and Y. Huang, *Nat. Nanotechnol.* **5**, 190 (2010); X. Liang, Y. S. Jung, S. Wu, and A. Ismach, *Nano Lett.* **10**, 2454 (2010); J. J. Ding, K. Du, I. Wathuthanthri, and C. H. Choi, *J. Vac. Sci. Technol. B* **32**, 06FF01 (2014).
- ¹⁹J. H. Warner, Y. Fan, A. W. Robertson, K. He, and E. Yoon, *Nano Lett.* **13**, 4937 (2013).
- ²⁰A. Rafsanjani and K. Bertoldi, *Phys. Rev. Lett.* **118**, 084301 (2017).
- ²¹Z. Song, C. Lv, M. Liang, and V. Sanphuang, *Small* **12**, 5401 (2016).
- ²²H. Qin, Y. Sun, J. Z. Liu, and Y. Liu, *Carbon* **108**, 204 (2016).
- ²³Z. Qi, D. K. Campbell, and H. S. Park, *Phys. Rev. B* **90**, 245437 (2014).
- ²⁴B. Mortazavi, A. Lherbier, Z. Fan, and A. Harju, *Nanoscale* **9**, 16329 (2017).
- ²⁵T. H. Vo, M. Shekhiriev, D. A. Kunkel, and M. D. Morton, *Nat. Commun.* **5**, 3189 (2014).
- ²⁶Y. W. Son, M. L. Cohen, and S. G. Louie, *Phys. Rev. Lett.* **97**, 216803 (2006); V. Barone, O. Hod, and G. E. Scuseria, *Nano Lett.* **6**, 2748 (2006).
- ²⁷H. Wang and M. Upmanyu, *Phys. Rev. B* **86**, 205411 (2012).
- ²⁸S. Plimpton, *J. Comput. Phys.* **117**, 1 (1995).
- ²⁹J. Zhang, J. Zhao, and J. Lu, *ACS Nano* **6**, 2704 (2012).
- ³⁰D. T. Ho, H. S. Park, and S. Y. Kim, *Nanoscale* **10**, 1207 (2018).
- ³¹Y. Wei, J. Wu, H. Yin, and X. Shi, *Nat. Mater.* **11**, 759 (2012); R. Grantab, V. B. Shenoy, and R. S. Ruoff, *Science* **330**, 946 (2010).
- ³²Z. G. Song, V. I. Artyukhov, J. Wu, and B. I. Yakobson, *ACS Nano* **9**, 401 (2015); T. Zhang, X. Li, and H. Gao, *J. Mech. Phys. Solids* **67**, 2 (2014).
- ³³D. W. Brenner, O. A. Shenderova, J. A. Harrison, and S. J. Stuart, *J. Phys. Condens. Matter* **14**, 783 (2002).
- ³⁴C. Wang, Y. Liu, L. Lan, and H. Tan, *Nanoscale* **5**, 4454 (2013).

- ³⁵H. Zhao and N. R. Aluru, *J. Appl. Phys.* **108**, 064321 (2010); B. Morris, M. Becton, and X. Wang, *Carbon* **137**, 196 (2018).
- ³⁶B. H. Kim, K. R. Lee, Y. C. Chung, and J. G. Lee, *J. Appl. Phys.* **112**, 044312 (2012).
- ³⁷T. Chang, *Phys. Rev. Lett.* **101**, 175501 (2008).
- ³⁸H. E. Troiani, M. M. Yoshida, G. A. C. Bragado, and M. A. L. Marques, *Nano Lett.* **3**, 751 (2003).
- ³⁹M. A. L. Marques, H. E. Troiani, M. Miki-Yoshida, and M. Jose-Yacamán, *Nano Lett.* **4**, 811 (2004).
- ⁴⁰O. Cretu, A. R. Botello-Mendez, I. Janowska, and C. Pham-Huu, *Nano Lett.* **13**, 3487 (2013).
- ⁴¹C. Jin, H. Lan, L. Peng, and K. Suenaga, *Phys. Rev. Lett.* **102**, 205501 (2009).
- ⁴²Y. Deng and S. W. Cranford, *Comp. Mater. Sci.* **129**, 226 (2017); A. K. Nair, S. W. Cranford, and M. J. Buehler, *EPL Europhys. Lett.* **95**, 16002 (2011).